J Mater Sci (2011) 46:5807–5814
DOI 10.1007/s10853-011-5536-2

Fabrication of crack-free SUS316L/Al_2O_3 functionally graded materials by spark plasma sintering

M. Radwan · M. Nygren · K. Flodström · S. Esmaelzadeh

Received: 15 October 2010 / Accepted: 5 April 2011 / Published online: 12 April 2011

Abstract This paper describes the preparation of crack-free stainless steel 316L/alumina functionally graded material (SUS316L/Al_2O_3 FGM) by spark plasma sintering (SPS). The sintering of individual powders and their composites was first studied to find an optimum SPS condition to get both materials and their mixtures highly dense. Sintering of cylindrical-shaped FGM pellets (ϕ20 mm) with various numbers of interlayers of 1, 2, 3, 4, and 9 was then carried out where the kind of and location of related cracking were carefully examined. The FGMs faced the problem of cracking mainly in the radial direction near the Al_2O_3-rich layers regardless of the number of layers or the gradient compositional profile. An yttrium-stabilized zirconia (3Y-ZrO_2) was added thereafter to the gradient on the expense of Al_2O_3 content (up to 50 vol.%) and no radial cracking was found. Defects-free FGM pellets were successfully produced by interposing 19 interlayers between the SUS316L and Al_2O_3 ends. The Vickers hardness profile was determined throughout the cross-section of sintered FGM and it was varying steadily through the gradient from 2.0 GPa at the SUS316L surface to 14.4 GPa at the Al_2O_3 surface.

M. Radwan (✉) · M. Nygren · S. Esmaelzadeh
Department of Material and Environmental Chemistry, Arrhenius Laboratory, Stockholm University, 106 91 Stockholm, Sweden
e-mail: mohamed.radwan@mmk.su.se

M. Radwan · K. Flodström · S. Esmaelzadeh
Diamorph AB, Roslagstullsbacken 11, 106 91 Stockholm, Sweden

Introduction

The concept of functionally graded materials (FGMs) is an ideal material design solution in engineering applications that require innovative materials with hybrid properties and/or functions which cannot be realized in a single homogeneous material or composite, or that need a solution to the problem of thermo-mechanical property mismatch at the interface in a junction between different materials. The general idea of graded materials was first proposed in 1972 [1, 2], while systematic development of the concept is owed to the research programs in Japan in the middle of 1980s [3, 4]. In its simplest architecture, a FGM is a structure or part that consists of one material on one side, a second material on the other side, and an intermediate region of graded composites whose composition changes gradually from one material to the other. Two dissimilar materials can thus be bonded in a structure where the properties change gradually with the location. This gradient is designed to obtain a thermal residual stress relaxation through the smooth variation of the compositions, morphologies, and properties along the structure. FGMs can be fabricated by various processing methods such as physical–chemical vapor depositions, thin sheet lamination, plasma spraying, sol–gel methods, self-propagating high-temperature synthesis (SHS), powder metallurgy routes, and spark plasma sintering (SPS) [5, 6]. The materials have been successfully used in a variety of low- and high-technology applications in transport systems, energy conversion systems, cutting and drilling tools, machine parts, semiconductors, optics, and bio-systems [7–10].

The structures of metal/ceramic FGMs have received much interest although ceramic/ceramic, metal/metal, and polymer-based FGMs are also fabricated [6]. One of the first metal/ceramic FGMs which was developed for

Japanese aerospace vehicle components was the austenitic stainless steel 304/zirconia (SUS304/PSZ) FGM as a thermal barrier material to bear the extreme heat flow during re-entry with a function to withstand the temperature differences in the order of 1000 K in structural components of about 10 mm thickness or less [7]. Similar metal/ceramic FGMs have been fabricated for other areas of applications, e.g., Ni/ZrO_2, Cu/TiB_2, Ni/TiC, WC/Co, and Ti/HAp based FGMs [6, 7, 9]. Modeling to develop a stainless steel/alumina (SUS/Al_2O_3) FGM system has been studied over the last years by Grujicic and Zhao [11], Matsuno et al. [12], Shinagawa [13], Pietrzak et al. [14], and Liu et al. [15] as potential structural components for applications in high wear resistance ceramic—heat resisting stainless steel joints and tritium penetration barriers (TPB). The effects of material properties, specimen geometry, and gradient compositional profile on the residual stress distributions during the cooling stage and the crack formation especially in the Al_2O_3-rich region have been well demonstrated. The SUS/Al_2O_3 FGM system encounters two major problems; the large thermo-mechanical property mismatch between the end components and the brittleness of Al_2O_3. According to numerical calculations of the residual stress concentration in some critical Al_2O_3-rich regions within the FGM specimen, these stresses could easily be in the same range as the bending or tensile strength of A_2O_3 (250–275 MPa) [11, 14, 15], which would make it difficult to fabricate FGM specimens without material defects. Still, there has been a need for systematic experimental studies to get close insight into this material combination and to find a viable procedure that could control the problem of residual stress-induced cracking.

In this study, the possibility to prepare stainless steel/Al_2O_3 FGMs has been evaluated. The experiments focused first on sintering the mono materials of austenitic stainless steel 316L (SUS316L) and Al_2O_3 as well as their composites in order to explore optimum sintering parameters to get the materials highly dense. Thereafter, sintering of pellet-shaped FGMs has been carried out with careful observation of the associated cracking problems. The compositions of the graded interlayers were determined using a modified rule-of-mixture power law equation (proposed by the first author based on the basic formula described in Refs. [11, 14, 15]) where the local volume fraction of SUS316L, V_i, in each interlayer was calculated as follows:

$$V_i = \left[1 - (i/n + 1)^P\right] \quad (1)$$

where i is the number of each layer, n is the total number of interlayers, and P is a material concentration exponent which shows how the concentration of the metal powder gradually changes through the n interlayers. As will be shown below, P and n were here varied, but no completely crack-free FGM could be produced. In order to reduce the thermal mismatch between the end components, the alumina in the interlayers was replaced by a mixture of Al_2O_3 and yttrium-stabilized zirconia, ZrO_2(3Y). Zirconia has intermediate thermo-elastic properties between those of SUS316L and Al_2O_3, implying that it can lower the residual stresses, and simultaneously acts as an enforcement component to strengthen the graded region.

The FGM pellets were fabricated by SPS, also called field assisted sintering technology (FAST), which is a relatively new sintering technique that allows consolidation of numerous advanced materials such as gradient materials, nano-structured materials, and composite materials [16]. The SPS process is a pressure assisted sintering technique and the pressure mold, referred to as die, is heated by allowing a pulsed DC current to pass through the mold, implying that very rapid heating rates can be applied. It is well known that short holding times and low sintering temperatures can be used [17].

Experimental procedure

The materials used in this study were stainless steel type Micro-Melt® 316L (Carpenter Powder Products Inc, USA), ultrapure α-alumina powder (TM-DAR, Taimei Chemicals Co., Ltd., Japan), and 3 mol.% Y_2O_3-doped zirconia powder (TZ-3Y, Tosoh Corporation, Japan). The main characteristics of the three powders are shown in Table 1.

Sinterability studies of the stainless steel and Al_2O_3 powders as well as their composites (20, 40, 60, and 80 wt% SUS316L) were first carried out to optimize the SPS sintering parameters. Thereafter, a series of sintering tests for pellet-shaped FGMs were performed. Appropriate amounts of powders for the composites and the FGM interlayers were manually mixed thoroughly to assure good homogeneity. The sintering experiments were carried out in vacuum in a SPS unit (SPS-5.40 MK-VI system, SPS Syntex Inc, Japan). Cylindrical graphite dies (outer diameter 50 mm, inner diameter 20.8 mm, height 50 mm, with punches of the size $\phi 20 \times 30$ mm) were used. A graphite sheet was used as a protecting layer between the inner wall of the die and the powder. For the FGMs, the mixtures of the layers were loaded in order, layer by layer into the graphite die, beginning with the pure alumina. The compositions of the graded interlayers were determined as described in Eq. 1.

Prior to the sintering, the samples were uniaxially pressed for 30 s using a pressure of 60 MPa. After sintering, the dense pellets were polished by SiC paper to remove the graphite residues. The relative densities of sintered specimens, ρ, were measured in deionized water

Table 1 Main characteristics of the starting powders used

Powder	Name	Average particle size (μm)	Density (g/cc)	CTE (10^{-6}/°C)	Chemical analysis (wt%)
Stainless steel 316L	Micro-Melt® 316L	<22	7.95	18.5 (649 °C)	0.03 C, 0.03 S, 0.045 P, 1.0 Si, 2.0 Mn, 2.0–3.0 Mo, 10.0–14.0 Ni, 16.0–18.0 Cr, 61.9–68.89 Fe
Alumina	Taimicron TM-DAR	0.1	3.98	4	99.99% Al_2O_3
Zirconia	Tosoh-Zirconia	–	6.05	10	Contains 3 mol.% Y_2O_3

by the Archimedes method (European Standard EN 993-1) and calculated as follows:

$$\rho = \frac{m_1}{m_3 - m_2}.\rho_w \quad (2)$$

where m_1 is the weight of the sample determined in air, m_2 is the weight of the sample completely immersed and saturated in water, m_3 is the weight of the saturated sample in air, and ρ_w is the density of deionized water defined for the specific temperature.

The occurrence of surface cracks in the sintered FGM pellets was examined visually and through optical microscopy (Olympus SZx12 model, Olympus Optical Co. Ltd., Japan). The microstructure of the sintered samples was recorded in a field emission scanning electron microscopy (FE-SEM, JSM-7000F, JEOL, Japan). One successful FGM sample was cut and the cross-section surface was polished with diamond slurries down to 1 μm. A Vickers diamond indenter (Vickers-Armstrongs Engineers Ltd., UK) was used to determine the hardness of the individual interlayers using a load of 98.1 N. The sizes of the indentations' diagonals were determined using SEM and the Vickers hardness was calculated according to the following equation:

$$H_v = 0.0018544\ (P/d^2) \quad (3)$$

where H_v is the Vickers hardness (GPa), P is the load (N), and d is the average length of the two diagonals of the indentations (mm).

Results and discussion

Sinterability of stainless steel 316L and Al_2O_3 powders

In this set of experiments, the focus was to explore an optimum SPS condition at which both SUS316L and Al_2O_3 could be made fully dense. Stainless steel can be sintered to high relative density by SPS in the temperature range of 900–1000 °C [18, 19], while the minimum reported SPS temperature to obtain fully dense Al_2O_3 was 1150 °C [20].

At first, the predetermined pressure was applied at room temperature and the samples were heated from room temperature to 600 °C in 3 min and then heated to the predetermined sintering temperature. The samples were thereafter held at this temperature for a certain holding time before turning off the power. Disc-shaped samples with a size of 20 mm in diameter and 4 mm in thickness were sintered.

In the case of stainless steel, boron nitride (BN) powder was placed as an insulating layer below and above the stainless steel powder in order to direct the current to flow mainly in the graphite die (not through the stainless steel sample) thus avoiding local heating effects. Figure 1 shows the effect of sintering temperature, holding time, and applied pressure on the relative density of sintered SUS316 specimens. A density of >98.5% can be obtained at 1000–1100 °C with 5–10 min holding time under 50–75 MPa pressure. Above 1100 °C, the SUS316L starts melting. The SPS temperature was monitored and regulated by an optical pyrometer focused on a small hole on the surface of the die, however, as is well known, the actual temperature of the sample is slightly higher than the measured one.

The sintering of Al_2O_3 was then carried out at 1100 °C under a pressure of 75 MPa and different holding times. The effect of holding time on the relative density of sintered Al_2O_3 samples is given in Fig. 2. Nearly fully dense Al_2O_3 samples (98.6%) could be produced at 1100 °C using a holding time of 30 min.

Sinterability of SUS316L–Al_2O_3 composites

A series of various compositions in steps of 20 wt% SUS316L were sintered at 1100 °C for 30 min under 75 MPa. Figure 3 shows the relative densities of the composites plotted as a function of the stainless steel content. Initially the relative density decreases with the increasing content of SUS316L, but around 40 wt% SUS316L (or 25 vol.% SUS316L) it gradually increases with increasing SUS316L. The microstructure of the composite containing 25 vol.% S316L is shown in Fig. 4. Figure 4a and b shows the microstructures of a polished surface and a polished cross-section, respectively. The content of stainless steel particles seems to be slightly

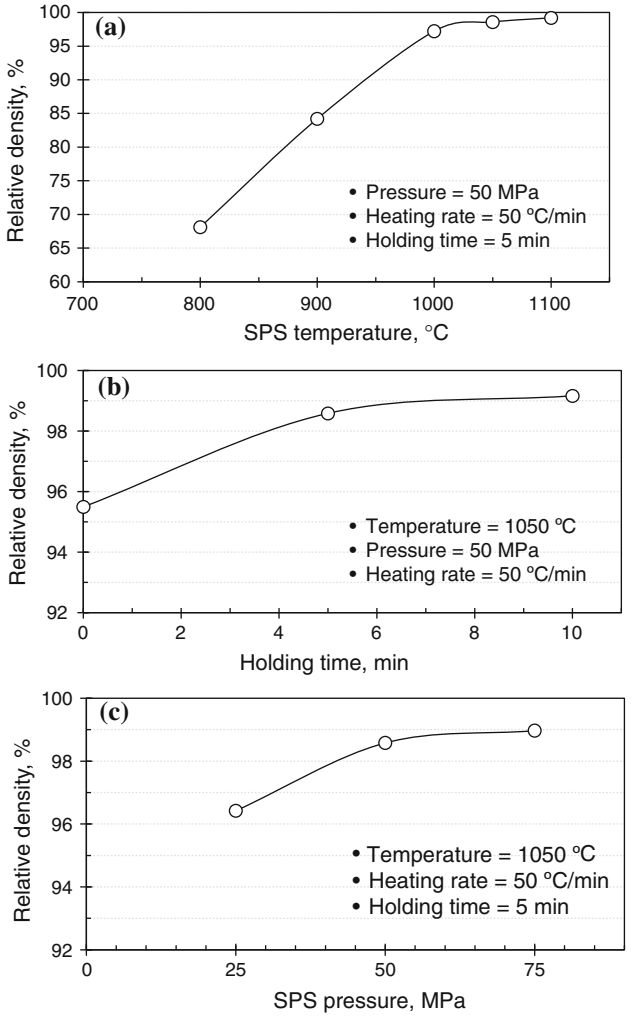

Fig. 1 Relative density of SPSed SUS316L specimens as function of temperature (**a**), holding time (**b**), and applied pressure (**c**)

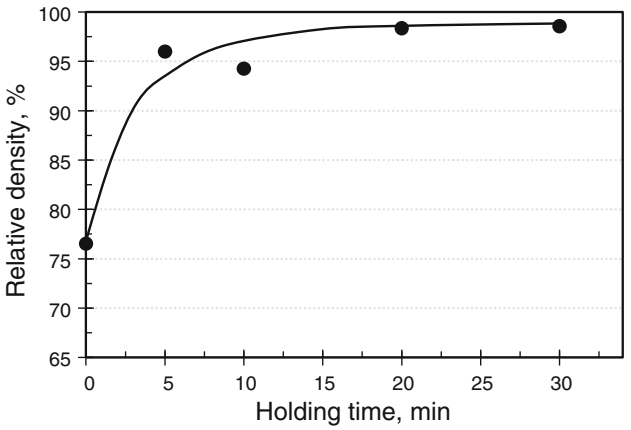

Fig. 2 Relative density as a function of holding time for Al_2O_3 SPSed at 1100 °C using a heating rate of 100°/min and a pressure of 75 MPa

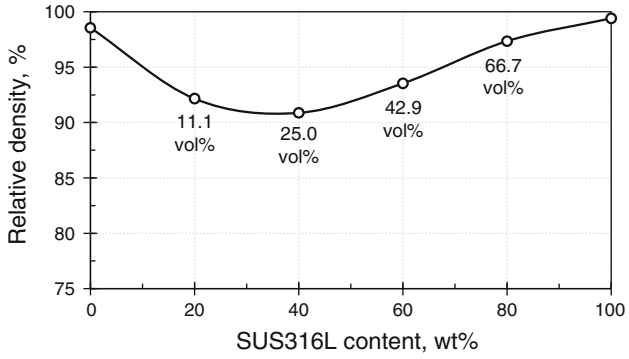

Fig. 3 Relative density of SPSed samples plotted versus the composition of sintered SUS316L–Al_2O_3 composites

higher at the surface than in the cross-section, and larger islands of Al_2O_3 are found in the latter section. Figure 4c shows the features of the Al_2O_3 matrix near a stainless steel particle, where residual stresses occur upon cooling due to the large mismatch in thermal expansion coefficients. Micro-porosity as well as some voids in the Al_2O_3 matrix and the stainless steel particles, respectively, can be observed.

Sintering of SUS316L/Al_2O_3 FGMs

Based on the above experimental results, FGM pellets with 1, 2, 3, 4, and 9 interlayers (i.e., $n = 1, 2, 3, 4$, or 9) having a linear compositional profile ($P = 1$) were sintered. The SPS parameters were: pressure 75 MPa, heating rate 100°/min, sintering temperature 1100 °C, and holding time 30 min. We found various interfacial defects in the sintered FGMs such as delamination or fracture of alumina, or radial cracking in gradient layers as seen in Fig. 5. In these samples, the FGM containing 9 interlayers exhibited fewer defects than the others.

The effect of composition profile through the interlayers was studied by varying the value of the exponent P in Eq. 1, setting P to 0.5, 0.75, 1.5, 1.8, 2.0, 3.0, and 4.0, while keeping $n = 9$. For a given value of P, the volume fractions of SUS316L and Al_2O_3 within each of the 9 interlayers were calculated from Eq. 1. In all samples, the thickness of the stainless steel layer was 2.0 mm, the thickness of the Al_2O_3 layer was 1.0 mm and the thickness of each interlayer was 1.0 mm. The results showed that the cracking in the FGM pellets can be minimized, as shown in Fig. 6. However, radial cracks were always found, located mainly at the interfaces close to the composition of 30 vol.% SUS316L–70 vol.% Al_2O_3, i.e., in the compositional area where the SUS316L–Al_2O_3 composite exhibited lowest density, see Fig. 3. Microstructural observation of the cross-section of one sintered FGM pellet with $P = 1$ and $n = 9$ is shown in Fig. 7. Radial cracks at the edge and

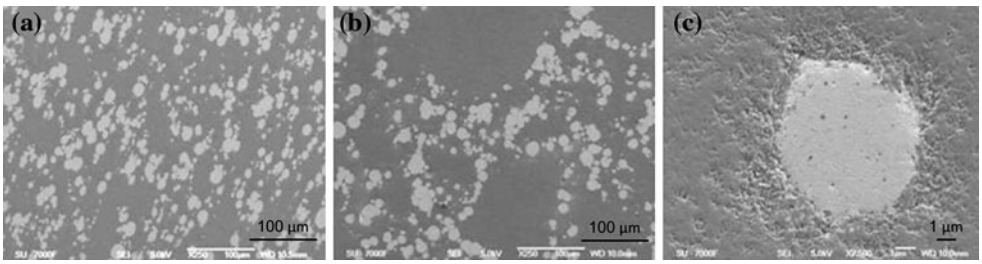

Fig. 4 SEM micrographs of 25 vol.%SUS316L–75 vol.%Al_2O_3 composite; **a** polished surface, **b** polished cross-section, and **c** features of Al_2O_3 matrix near a SUS316L particle

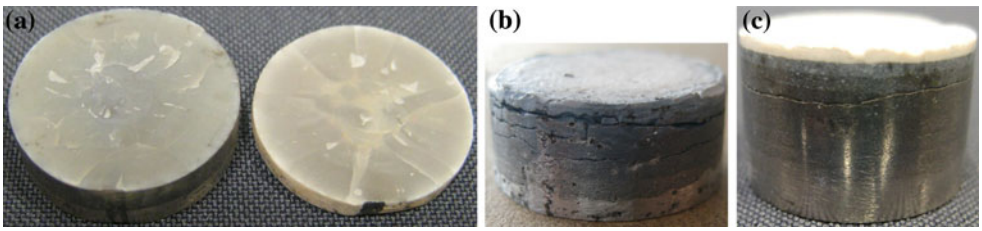

Fig. 5 Examples of cracking in sintered FGM specimens with various interlayers; **a** having 1 interlayer (the Al_2O_3 layer piled off), **b** having 4 interlayers, and **c** having 9 interlayers

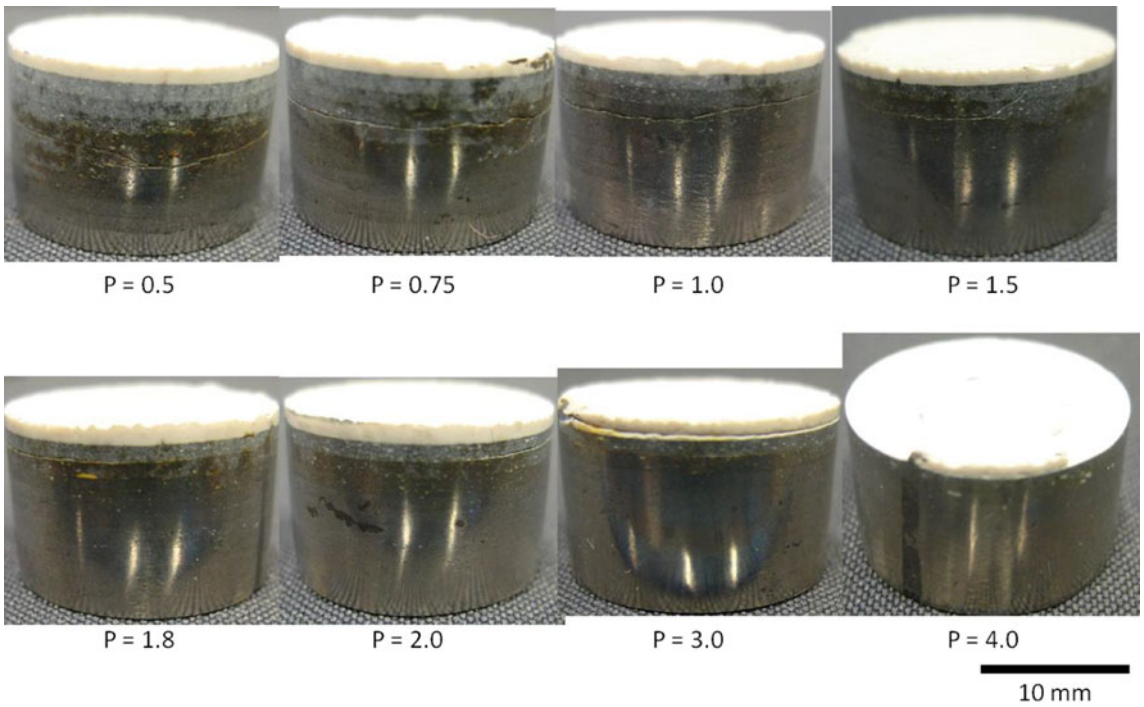

Fig. 6 Optical photographs show radial cracking in SPSed FGM pellets having various *P* values

in the center of the sintered specimen were observed. The crack width was larger near the edge than at the center of the sample which is in agreement with the modeling of residual stresses in Ref. [11].

The magnitudes of the residual stresses throughout the FGM will depend on the extent of thermal strains that occur both on a microstructure-level (at the particle–particle interface) and on a macrostructure-level (between

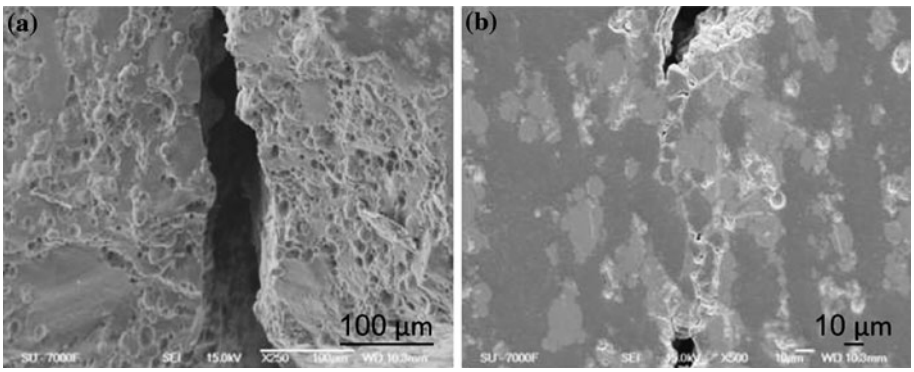

Fig. 7 SEM micrographs of the radial crack in SPSed SUS316L/Al_2O_3 FGM sample; **a** at edge, and **b** in the center ($n = 9$ and $P = 1$)

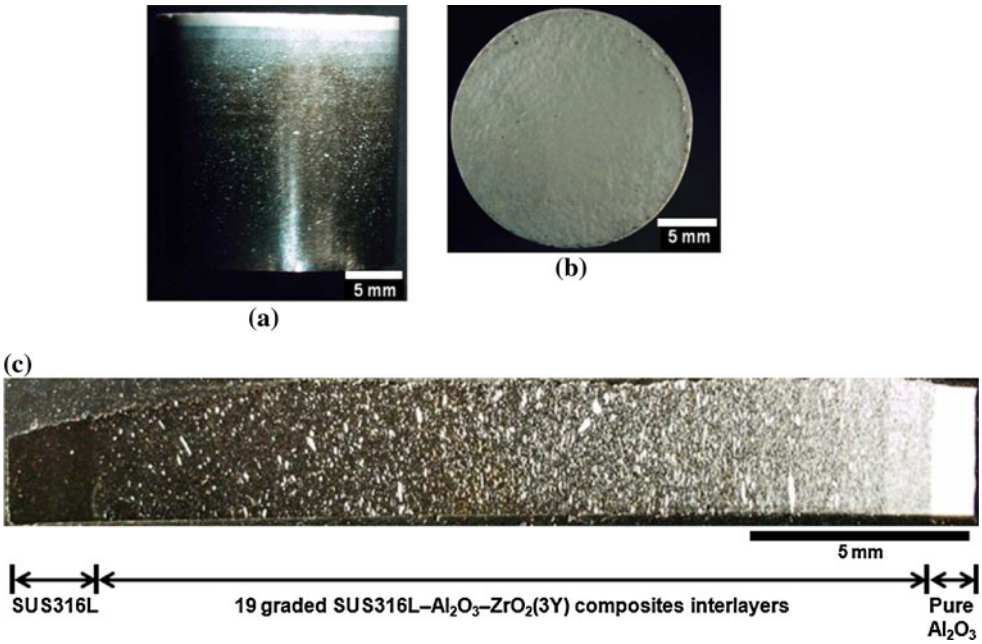

Fig. 8 Optical photographs showing **a** the sintered SUS316L/Al_2O_3 FGM sample, **b** a top-view of the Al_2O_3 layer, and **c** cross-section of the multilayer structure

adjacent layers) during the cooling as can be generally described by the following basic equation:

$$\sigma = E\,\Delta\alpha\,\Delta T \tag{4}$$

where σ is the residual thermal stress (MPa), E is the Young's modulus (MPa), $\Delta\alpha$ is the thermal expansion mismatch (cm/cm/°C), and ΔT is the difference between the sintering temperature and room temperature (°C).

According to Eq. 4, the best solution to reduce the residual thermal stresses, σ, lies in minimizing the thermal expansion mismatch, $\Delta\alpha$, between the phases and the sintering temperature, meanwhile improving the mechanical toughness of the matrices especially in the composition range where the maximum thermal stresses arise.

Commercial submicron or micron-sized Al_2O_3 powder is usually sintered by SPS in the temperature range of 1400–1700 °C [21]. In this work, a commercial nano-sized Al_2O_3 powder with high sinterability was chosen so that using the sintering parameters given above (1100 °C/30 min/75 MPa) yielded a compact with a relative density of 98.6%. 1100 °C is the critical maximum temperature, as the SUS316L starts melting above this temperature. The ΔT value given in Eq. 4 is thus reduced to ~1100 °C.

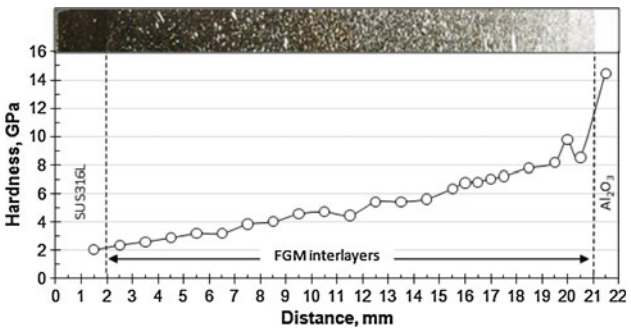

Fig. 9 The Vickers hardness profile throughout the cross-section of crack-free SUS316L/Al_2O_3 FGM pellet

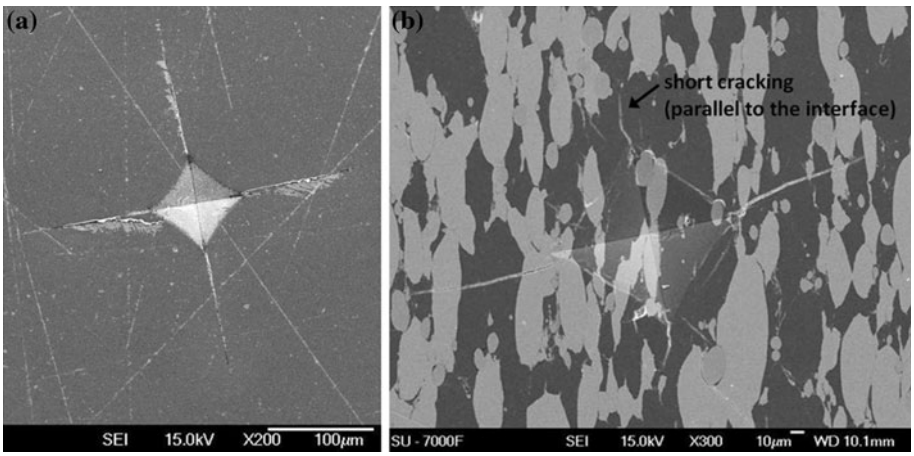

Fig. 10 SEM micrographs of the cracks developed in connection with the Vickers indentation tests using a load of 98.1 N **a** monolithic dense Al_2O_3, and **b** SUS316L/Al_2O_3 FGM

The thermal expansion coefficient of Al_2O_3 ($\alpha_{Al_2O_3} \approx 6 \times 10^{-6}/^{\circ}C$) is much lower than that of SUS316L ($\alpha_{SUS316L} \approx 18 \times 10^{-6}/^{\circ}C$). Reducing the thermal expansion mismatch, $\Delta\alpha$, and achieving reinforcement of the Al_2O_3 layers were accomplished further by the addition of adequate amounts of ZrO_2(3Y) into the SUS316L–Al_2O_3 composite layers. ZrO_2(3Y) has an intermediate coefficient of thermal expansion ($\alpha_{ZrO_2} \approx 10 \times 10^{-6}/^{\circ}C$), large bending strength ($\sim$900 MPa) and high fracture toughness (6–10 MPa $m^{1/2}$). In the ceramic-rich region, the addition of ZrO_2(3Y) reduces the thermal expansion mismatch and improves the mechanical properties of the composite layers. Thus, in a set of experiments, Al_2O_3 was replaced by 25, 30, 40, 45, and 50 vol.% of ZrO_2(3Y), respectively, in all interlayers. The results showed that the radial cracking decreased while increasing the zirconia content in the interlayers. For ZrO_2(3Y) contents $\geq$40 vol.%, no radial cracks were found. However, tiny axial cracking developed in the pure alumina layer during polishing of the sample. This problem was solved by increasing the number of interlayers to 19 layers. Photos of the FGM pellet, the pure Al_2O_3 layer, and the cross-section of the gradient are given in Fig. 8. No delamination or internal cracking could be observed. The relative density of that sintered FGM pellet was $\sim$95% as measured by the Archimedes method.

The Vickers hardness profile along the cross-section of the successful crack-free FGM is plotted as a function of the distance in Fig. 9. The hardness values increase steadily with decreasing stainless steel content. Figure 10 shows the crack patterns generated by the Vickers' indentations on a monolithic Al_2O_3 sample and in the 19th layer (adjacent to pure Al_2O_3 layer) close to the 18th layer. The SEM images show that the length of the cracks parallel to the interface, for the composite layer, was markedly shorter than those normal to the interface, while, in the pure Al_2O_3 the size of the cracks from the four corners was very similar. This behavior is a direct evidence of the existence of a compressive stress in the direction normal to the interface. Under fairly high compressive stresses, ZrO_2(3Y) may withstand a transformation from a tetragonal to a monoclinic modification which might enhance the fracture toughness of the relevant layer according to a transformation toughening mechanism as previously illustrated by other research groups [22–24].

Conclusions

A highly dense, crack-free, stainless steel type 316L, and alumina FGM (SUS316L/Al_2O_3 FGM) was fabricated successfully from powders by a simple SPS process. The densification of mono materials as well as their composite mixtures was first conducted, in order to get a good understanding of the material system. The successful FGM specimen, 20 mm in diameter and 21 mm high, consisted of 19 graded interlayers having various fractions of SUS316L, Al_2O_3, and yttrium-stabilized zirconia (ZrO_2 (3Y)), placed between the pure SUS316L and Al_2O_3 end surfaces. The success to fabricate crack-free SUS316L/Al_2O_3 FGM pellets is believed to be attributed to the following reasons: (1) using a nano-Al_2O_3 powder that can be sintered at a low temperature by SPS, (2) adding ZrO_2(3Y) into the graded interlayers as a toughening phase, and (3) interposing a sufficient number of interlayers between the pure SUS316L and Al_2O_3 layers to decrease the differences in the thermal expansion mismatches between the adjacent layers.

References

1. Shen M, Bever MB (1972) J Mater Sci 7:741. doi: 10.1007/BF00549902
2. Bever MB, Duwez PE (1972) Mater Sci Eng 10:1
3. Kawasaki A, Watanabe R (1987) J Jpn Inst Met 51:525

4. Niino M (1990) J Jpn Soc Powder Powder Metall 37:241
5. Kieback B, Neubrand A, Riedel H (2003) Mater Sci Eng A632:81
6. Watanabe R, Nishida T, Hirai T (2003) Met Mater Int 9:513
7. Ilschner B (1993) J Phys IV 3:763
8. Cherradi N, Kawasaki A, Gasik M (1994) Compos Eng 4:883
9. Miyamoto Y, Kaysser WA, Rabin BH, Kawasaki A, Ford RG (1999) Functionally graded materials: design, processing and applications. Kluwer Academic Publishers, Boston
10. Niino M, Kisara K (2004) J Jpn Soc Powder Powder Metall 51:242
11. Grujicic M, Zhao H (1998) Mater Sci Eng A252:117
12. Matsuno S, Inomoto H, Ameyama K (2000) In: Proceedings of powder metallurgy world congress exhibition 2000, p 745
13. Shinagawa K (2000) Computer aided design of graded powder compacts to control sintering defects, Functionally Graded Materials in the 21st Century. A Workshop on Trends and Forecasts, Tsukuba, Japan
14. Pietrzak K, Kaliński D, Chmielewski M (2007) J Eur Ceram Soc 27:1281
15. Liu H, Tao J, Gautreau Y, Zhang P, Xu J (2009) Mater Des 30:2785
16. Orrù R, Licheri R, Locci AM, Cincotti A, Cao G (2009) Mater Sci Eng R 63:127
17. Tokita M (1997) In: Proceeding of the international symposium on microwave, plasma and thermomechanical processing of advanced materials, Osaka University, Japan, p 69
18. Hong-wei N, Hang H, Guang-qiang L, Jing L (2008) J Iron Steel Res Int 15:73
19. Xu Z, Jia C, Kuang C, Chu K, Qu X (2009) J Alloys Compd 484:924
20. Kim B, Hiraga K, Morita K, Yoshida H (2007) Scr Mater 57:607
21. Gao L, Hong JS, Miyamoto H, Torre SDDL (2000) J Eur Ceram Soc 20:2149
22. Tokita M, Kawahara M, Mizuuchi K, Makino Y (2009) J Jpn Soc Powder Powder Metall 56:383
23. Hong C, Zhang X, Li W, Han J, Meng S (2008) Mater Sci Eng A498:437
24. Zhang X, Li W, Hong C, Han W, Han J (2008) Scr Mater 59:1214